Journal of Robotics and Control (JRC)
Volume 5, Issue 5, 2024
ISSN: 2715-5072, DOI: 10.18196/jrc.v5i5.23379

Momentum-Based Push Recovery Control of Bipedal Robots Using a New Variable Power Reaching Law for Sliding Mode Control

Ibrahim Al-Tameemi [1*], Duc Doan [2], Abizer Patanwala [3], Mahdi Agheli [4]
[1, 2, 3, 4] Department of Robotics Engineering, Worcester Polytechnic Institute, Worcester, USA
Email: [1] ialtameemi@wpi.edu, [2] tvdoan@wpi.edu, [3] apatanwala@wpi.edu, [4] mmaghelih@wpi.edu
*Corresponding Author

***Abstract*—A significant challenge in deploying bipedal robots for human-oriented real-world applications is their ability to maintain balance when externally disturbed. Current momentum-based balance control strategies often exhibit inadequate robustness to disturbances due to reliance on simple proportional controllers and imprecise incorporation of desired angular momentum changes. Furthermore, the sequential activation of momentum and posture correction controllers compromises system stability when confronted with consecutive disturbances. This paper proposes and validates a new Variable Power Reaching Law for Sliding Mode Control (SMC) to enhance the regulation of linear momentum against disturbances. The proposed reaching law adjusts dynamically to the system's errors, ensuring fast convergence and minimal chattering. In this paper, we precisely define the desired angular momentum change in relation to the Center of Pressure (CoP), a crucial stability metric, as well as the desired linear momentum and ground reaction forces. The null-space method, which allows for simultaneous task execution by using unused degrees of freedom, is employed to ensure effective balance and upright posture without interference. The posture correction control is projected onto the null-space of momentum control. Simulation results confirm that the proposed control system effectively stabilizes the robot against external disturbances, regulating momentum and restoring upright posture. The null-space method proves effective in maintaining balance under multiple disturbances by simultaneously controlling momentum and posture. Comparative evaluations show that our approach outperforms traditional momentum-based controls and nonadaptive reaching laws, reducing CoP fluctuations, managing disturbances up to 117 N, and minimizing chattering and steady-state error. These advancements underscore the potential for deploying bipedal robots in dynamic environments.**

***Keywords*—Push Recovery; Dynamic Stability; Bipedal Robots; Sliding Mode Control; Null-Space Method; Center of Pressure.**

I. INTRODUCTION

Bipedal robots play a major role in many fields, like industrial automation, search-and-rescue missions, and healthcare services [1]. The ability of these robots to navigate over complex environments designed for human beings, such as stairs and uneven terrain, making them efficient for applications where wheeled robots fail to perform tasks in these conditions. One of the significant limitations that these robots face when conducting the aforementioned applications is the ability to maintain balance while experiencing external disturbances, such as pushes or uneven ground surfaces. Therefore, there is still a high need to develop push recovery control methods, which are important for the practical deployment of bipedal robots in real-world environments where unpredictability is common.

Previous studies conducted on the standing balance of a bipedal robot can be classified into two types of control schemes: joint control strategies and whole-body motion control methods. Joint control strategies involve using particular joints, such as the ankle, hip, or knee, to react and respond to disturbances [2]-[11]. The ankle strategy includes using the robot's ankle joint to effectively control disturbances, while keeping the other joints immobile. The Linear Inverted Pendulum Model is often adopted to develop an ankle-based push recovery control system. This strategy can only handle minor disturbances, as the ankle joints produce a restricted amount of torque. As an alternative, some researchers have concentrated on using the hip strategy, which is effective when dealing with relatively higher disturbances, while the ankle strategy alone is insufficient for maintaining balance. The objective of the hip strategy is to produce angular momentum that is complementary to the angular momentum caused by an external disturbance. The Center of Mass (CoM) of the robot is pushed towards the support polygon area by the angular momentum that is created around the hip. The Linear Inverted Pendulum Model, which incorporates a hip-mounted flywheel, is frequently utilized to describe the dynamics in the hip strategy. The hip strategy assumes that the CoM is precisely located at the hip joint, which is not typical in the majority of bipedal robots. This assumption simplifies the control problem but may result in inaccuracies in balance and motion control.

On the contrary, numerous studies have investigated the use of whole-body motion in bipedal robots to preserve standing stability. The literature has presented several whole-body balance control methods of bipedal robots [12]-[29], one of which is momentum-based balance control. This method focuses on regulating linear momentum, angular momentum, or both in order to attain stability when standing. Prior to the research conducted by Popovic and his colleagues in [30], momentum-based balance control studies primarily focused on regulating linear momentum. [30] emphasized the significance of efficiently controlling angular momentum to maintain balance. The Centre of Pressure (CoP) is the specific location where the resultant ground reaction forces (F_{GR}) are

concentrated. A bipedal robot achieves stability when its CoP remains inside the bounds of the support polygon. It was noted that the location of the CoP has a non-linear correlation with both the force (F_{GR}) and the CoM position. Therefore, in order to have complete control over the CoP, it is essential to stabilize both linear and angular momentum.

In [21] derived the motion equation of the humanoid robot in relation to the combined linear and angular momentum. The total momentum is a six-dimensional vector that characterizes the macroscopic behavior of the complete robot. In [21], the desired momenta were first defined using a simple proportional- derivative (PD) controller, and then the joint velocities corresponding to these desired momenta were computed using the Centroidal Momentum Matrix (CMM). However, the stability criteria—which include keeping the CoP position within the support region—were neglected, so the robot could become unstable when the input momenta values are high. The authors of [22], [23] included the CoP position in the definition of the desired momenta. In [23], the authors used the CoM and CoP position errors to define the desired rate of change of angular momentum. In [22], the admissible values of F_{GR} and CoP positions which correspond to the desired momenta were determined. Then, the admissible rate of changes in momenta was calculated using the admissible F_{GR} and CoP position values. CMM was subsequently employed to calculate the necessary joint accelerations in accordance with the momenta rate of change.

In [13] created a balance control that compensates for the external pushing force by adjusting the foot contact force. The external forces in all axes were estimated using the centroidal dynamics and sensor measurements obtained from the Inertia Measurement Unit (IMU) and foot force sensors. Subsequently, an optimization problem is formulated to compute the optimal contact forces necessary to achieve the desired momenta. In [14], the authors introduced a model-based approach known as Dynamic Balance Force Control (DBFC) to compute the whole-body joint torques. The contact forces that control the rate of change of linear and angular momentum were established via an optimization problem with CoP position constraint. However, because the balancing stability problem assumed a zero desired rate of change of angular momentum, it did not incorporate the contribution of angular momentum.

The study conducted in [20] employed the PD controller to define the desired rate of change of angular momentum in terms of CoP position and velocity. A multi-objective optimization technique was formulated in [20] to obtain feasible joint accelerations with varying weights for linear and angular momentum terms. In cases where it was not feasible to achieve both desired momenta, a higher priority was given to the linear momentum [20], [24]. Insufficient rotational stability is the consequence of prioritizing linear momentum over angular momentum.

In [23], the two main phases of balancing were defined: the reflex phase, which involves promptly reacting to external forces by adjusting the rate of momentum changes using a simple proportional controller, and the recovery phase, which tries to return the robot to an upright position. A maximization optimization problem was developed to obtain the control law for the recovery phase, with the objective of maximizing the potential energy. In [23], the reflex and recovery phases were carried out sequentially. If a push happens during the recovery phase, the reflex phase, which regulates momenta, will not be triggered. Consequently, the robot behaves like a stiff pendulum, causing the CoP to move outside the area of support and losing stability.

Despite the advancements, there are still some limitations that need to be addressed to allow bipedal robots to effectively conduct real-world tasks in the presence of disturbances. Several previous studies used simple proportional controllers to regulate linear momentum, but these controllers may not offer enough robustness against disturbances. Furthermore, the desired rate of change of angular momentum was either presumed to be zero or it lacked the ability to adequately incorporate crucial components such as CoP, ground reaction forces, and desired linear momentum. This results in inadequate coordination between the upper and lower parts of the robot, making it challenging to maintain balance when subjected to disturbances. The bipedal robots' inability to maintain stability when subjected to multiple pushes is a result of dividing the balance control into two separate phases: one for regulating desired momenta and the other for posture control, and performing them sequentially.

This paper's contributions are threefold, each addressing critical gaps identified in the existing literature. First, we develop and validate a new reaching law for Sliding Mode Control (SMC) to stabilize the linear momentum of bipedal robots. The proposed reaching law uses variable power that adapts dynamically to changes in the system, guaranteeing minimal chattering and rapid convergence time to the sliding surface. Second, our research successfully manages the angular momentum by generating the desired rate of angular momentum change around the CoM, taking into account important factors such as the desired linear momentum, the position of the CoP, and the ground reaction forces. This definition, based on the principles of balance, assists in properly calculating the necessary angular momentum in the presence of external disturbances. Third, we use the null-space method to execute momentum and posture recovery controllers simultaneously, without any interference. By employing the null-space method, our bipedal robot can effectively regain its balance and return to an upright position, even when faced with several consecutive disturbances.

The remainder of this paper is organized as follows: Section II provides a detailed description of the methodology used in developing the proposed push recovery controller. Section III presents the results of the proposed controller, including comparisons with previous studies. Finally, Section IV presents conclusions and outlines future work.

II. METHODOLOGY

A. Robot Model

Our robot, HURON, is a lower body of a humanoid robot designed after human anatomy, with two lower limbs, including hips, thighs, shins, and feet. The robot is manufactured where all components are rigid and

interconnected via electric- actuated revolute joints (see Fig. 1). It weighs about 40 kg, stands 1.2 m tall, and provides 12 Degrees of Freedom (DoF) when both feet are flat on the ground—six on each limb, including hip joint roll, pitch, and yaw, knee joint pitch, and ankle joint roll and pitch. Additionally, the robot is equipped with force sensors to measure F_{GR}, necessary for calculating CoP position.

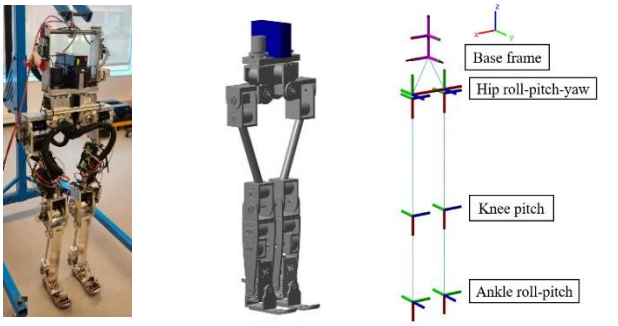

(a) (b) (c)

Fig. 1. HURON lower body. (a) physical robot, (b) simulation model, (c) robot frames

B. Mechanics of Balance

In the absence of external disturbances, the standing bipedal robot's momentum results solely from F_{GR} and gravitational forces. F_{GR} is $[F_{GRx}, F_{GRy}, F_{GRz}]^\top$ applied to the CoP, p is the CoP position $[p_x, p_y, 0]^\top$, and c is the CoM of the robot $[c_x, c_y, c_z]^\top$. The rate of change of the angular momentum about CoM in the sagittal plane, under the influence of a horizontal pushing force, as shown in Fig. 2, results in (1).

$$\dot{H}_{CoM,y} = \sum \tau_{CoM,y} = (p_x - c_x)F_{GRz} + c_z F_{GRx} - u_z F_{pushing} \quad (1)$$

where u_z is the location of the pushing force with respect to CoM. Replacing F_{GRx} and F_{GRz} with their equivalent linear momentum terms, we obtain (2).

$$p_x = c_x + \frac{\dot{H}_{CoM,y} - c_z \dot{L}_x}{\dot{L}_z + mg} + \frac{u_z F_{pushing}}{\dot{L}_z + mg} \quad (2)$$

Equation (2) implies that when a positive pushing force is applied, p_x shifts forward, moving toward the edge of the foot as the force magnitude increases. To prevent the robot from tipping in a clockwise direction, for instance, it's necessary to apply a clockwise $\dot{H}_{CoM,y}$ [23]. Accordingly, this paper's balance control approach focuses on adjusting both CoM and CoP by regulating linear and angular momenta.

C. Disturbance Absorption Phase

The objective of this phase is to generate $\dot{H}_{CoM,y}$ to absorb the disturbance while regulating the CoM via the proposed reaching law-based Sliding Mode Control (SMC).

1) Linear Momentum Controller: Controlling the robot's linear momentum, equivalent to control the CoM motion as per Newton's laws, is achieved in this paper through an SMC. SMC is a robust control method that has been extensively employed in robotic control systems because of its ability to effectively handle uncertainties and external disturbances. Its application spans from legged robot systems, where the challenges of dynamic stability and adaptable locomotion are common [31]-[36], to robotic manipulators, which require high precision control and reliability to various operational conditions [37]-[43]. SMC involves two main elements: reaching and sliding [44]. The sliding phase's reaching condition is usually expressed as $s\dot{s} \leq 0$. The typical switching function s is given by (3).

$$s = \dot{e} + \lambda e \quad (3)$$

where λ is a nonzero constant, that determines the chattering level and reaching time, and e, $\dot{e}$ are the error in the CoM position and velocity, respectively.

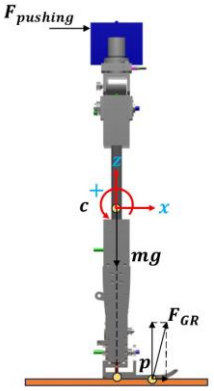

Fig. 2. A disturbing force applied to the robot

The generalized forces τ should be designed to derive the system to the equilibrium point, and the sliding condition $s\dot{s} \leq 0$ should be satisfied for all time. The sliding condition indicated above can be satisfied by developing a reliable reaching law, which is the differential expression of s. Nevertheless, it is crucial to acknowledge that the SMC does have its limitations. The occurrence of an undesired behavior known as chattering arises due to the non-instantaneous transition between the reaching and sliding phases. Chattering is characterized by rapid, high-frequency oscillations in the control signal. Excessive wear and tear on mechanical components, increased control effort, and noise generation may result from these oscillations. Thus, several studies [45]-[59] have been undertaken to examine the SMC with reaching laws, which was initially proposed by Gao and Hung [60].

The reaching law-based SMC proposed by Gao and Hung [60] includes different types: the Constant Rate Reaching Law (CRRL) and the Constant Power Reaching Law (CPRL). The Constant Rate Reaching Law can be mathematically represented as $(\dot{s} = -k\, sgn(s))$, where k is a positive constant gain. Raising k shortens the time it takes to reach the sliding surface, but it also makes the control action aggressive (quick response to minimize the system errors), which causes chattering. The Constant Power Rate Reaching Law is expressed as $(\dot{s} = -k\,|s|^{\rho} sgn(s))$, where k and ρ are constant and positive parameters. The reduction of the

parameter ρ has the potential to mitigate chattering phenomena; nevertheless, it is necessary to note that this adjustment may result in an increase in the time required to accomplish the desired outcome. Therefore, to mitigate the chattering phenomenon and simultaneously enhance the rate at which the sliding mode is approached, this study proposes the improved reaching law-based SMC designed to regulate the linear momentum or CoM motion.

The proposed reaching law for SMC is the Variable Power Rate Reaching Law ($\dot{s}$), which utilizes a variable power function, denoted as ($\delta\ (s)$). The variable power is a function that increases exponentially with the system state s. The Variable Power Rate Reaching Law is as follows,

$$\dot{s} = -k_1\ |s|^{\delta} sgn(s) \tag{4}$$

where the variable power ($\delta\ (s)$) is

$$\delta\ (s) = k_3(1 - e^{-\sigma|s|^{\eta}}), \qquad \delta\ (s) \in [0, k_3] \tag{5}$$

and k_1, k_3, σ, η are strictly positive parameters. Analyzing the Variable Power Rate Reaching Law ($\dot{s}$) presented in (4) reveals that the controller can adapt dynamically to changes in the switching function, as shown in Fig. 3. As $|s|$ grows, the variable power $\delta\ (s)$ tends toward k_3, implying that the further the sliding mode state s is to the equilibrium state, the more quickly it approaches, as shown in Fig. 3. If $|s|$ goes down, the Variable Power Rate Reaching Law ($\dot{s}$) gets closer to zero at a slower rate as the variable power $\delta\ (s)$ approaches a small value close to 0. This behavior indicates that the variable power $\delta\ (s)$ decreases as s approaches the equilibrium state, and chatter hardly occurs. Therefore, the proposed Variable Power Reaching Law can successfully resolve the problem of chattering and accelerate the rate at which the system reaches the sliding surface. Additionally, σ and η are included into the variable power function $\delta\ (s)$ to enhance adaptability, enabling accurate fine-tuning. σ effects the steepness of the exponential decay, while η enhances the sensitivity $\delta\ (s)$ to variations in the system state (s).

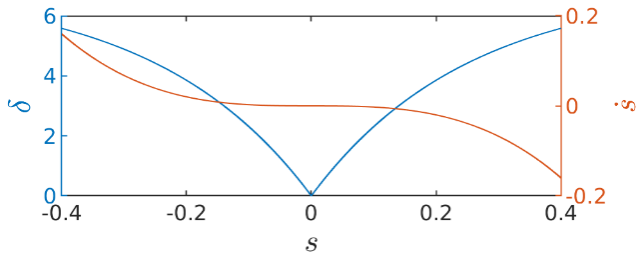

Fig. 3. System state s versus reaching law $\dot{s}$ and variable power δ

Theorem 1. The stability condition holds for the reaching law given by (4).

Proof. A Lyapunov function is considered:

$$V = \frac{1}{2}s^2 \tag{6}$$

Integrating (4), the time derivative of V is represented by

$$\dot{V} = s\dot{s} = -k_1\ |s|^{\delta} sgn(s)s \tag{7}$$

$$\dot{V} = s\dot{s} = -k_1\ |s|^{\delta+1} \tag{8}$$

where $k_1 > 0$, and then $\dot{V} < 0$, and the stability condition is satisfied. This means that the system state s will converge to the sliding surface ($s = 0$) and remain on it, leading to the desired CoM motion against disturbances.

The Double-Exponential (DE) transformation and trapezoidal rule [61]-[63] are used in this paper to perform numerical integration to determine the time required to reach the sliding surface $s = 0$. The MATLAB implementation yields finite reaching times, t_r, during which the system reaches $s = 0$ irrespective of the initial state value of s.

Since this study focuses on sagittal pushes, where the robot is standing (Double Support Phase), the lower body of HURON is simplified as a triple-inverted pendulum model ($n = 3$). By substituting (4) along with the acceleration kinematics, $\ddot{c}_x = J_x\ddot{q} + \dot{J}_x\dot{q}$ into the derivative of the typical sliding surface, $\dot{s} = \ddot{e} + \lambda\dot{e}$, we obtain the following equation:

$$-k_1|s|^{\delta} sgn(s) - \lambda\dot{e} = J_x\ddot{q} + \dot{J}_x\dot{q} \tag{9}$$

where $J_x \in \mathbb{R}^{1\times n}$ is the Jacobian matrix related to the linear velocity of the CoM along x-axis.

2) Angular Momentum Controller: This section focuses on generating a counteracting $\dot{H}_{CoM,y}$ to control the CoP according to (2). The angular momentum about the CoM is defined by

$$H_{CoM,y} = A(q)\dot{q} \tag{10}$$

where $H_{CoM,y}$ is the angular momentum of the robot about the CoM around the y-axis, $A(q)$ is $3 \times n$ inertia matrix and a function of q and its calculation is available in [21]. Because only the angular momentum about the y-axis is computed, $A(q)$ is reduced to $1 \times n$. Taking the time derivative of (10), we obtain

$$\dot{H}_{CoM,y} = \dot{A}\dot{q} + A\ddot{q} \tag{11}$$

The desired $\dot{H}_{CoM,y}$ is defined through two approaches:

First Approach: It is evident in the mechanics of balance that the absence of intersection between the CoP and CoM results in the generation of angular momentum around the CoM. Hence, the desired rate of change of angular momentum is defined by

$$\dot{H}_{CoM,y} = -k_H(p_x - c_x) \tag{12}$$

where k_H is a positive tuning parameter. This parameter amplifies the influence of the difference between CoP and CoM on the generation of the desired $\dot{H}_{CoM,y}$.

Second Approach: In this approach, the third term of (2) is eliminated under the assumption that both the magnitude

and position of the pushing force are unknown. In addition, the F_{GRx} is substituted by the linear momentum controller suggested in this paper. The desired $\dot{H}_{CoM,y}$ is defined as follows:

$$\dot{H}_{CoM,y} = -k_H[(p_x - c_x)F_{GRz} - c_x(-m(\dot{s} - \lambda\dot{e}))] \quad (13)$$

The desired $\dot{H}_{CoM,y}$ is determined by applying the principles of balance (2), which takes into account all significant factors that influence the desired $\dot{H}_{CoM,y}$. Consequently, we believe that this method allows for the calculation of a precise value of the desired $\dot{H}_{CoM,y}$ around the CoM to counteract the momentum produced or induced by the pushing force.

3) Combination of Momentum Controllers: The objective in this phase is to generate $\dot{H}_{CoM,y}$ to absorb the pushing force while regulating the CoM via the proposed SMC. By solving (9) and (11) simultaneously with the Moore-Penrose pseudoinverse, we obtain the joint accelerations $\ddot{q}$ that satisfy the linear and angular momentum controllers as

$$\ddot{q}_{momentum} = \begin{bmatrix} J_x \\ A \end{bmatrix}^{\dagger} \begin{bmatrix} -K_1|s|^{\delta}sgn(s) - \lambda\dot{e} - \dot{J}_x\dot{q} \\ \dot{H}_{CoM,y} - \dot{A}\dot{q} \end{bmatrix} \quad (14)$$

D. Posture Recovery Phase

For complete push recovery, a "posture task" is essential to return the robot to an upright position. However, integrating this task with momentum control can create conflicts [23]. In the case of a redundant robot (the number of joints exceeds the number of tasks), resolving this challenge entails utilizing extra DoF to adjust the robot's behavior without affecting the primary task or causing conflicts.

In robotic control, the null-space method has been substantially employed to facilitate the execution of multiple tasks simultaneously with minimum interference by applying the hierarchy of task priorities [64]-[70]. This method involves projecting lower priority tasks into the null space of higher-priority tasks, ensuring that the lower-priority tasks do not interfere with the higher-priority ones. Various generalized frameworks for managing tasks with prioritization have been developed at different levels, including velocity [71]-[73], acceleration [74], [75], and torque [76]-[79]. The characteristics of these different approaches are discussed in [80]. Our aim is to simultaneously perform both the higher-priority momentum task and the lower priority posture recovery task with minimal conflicts. In our push-recovery application, where the task dimension (two) is less than the number of joints (three), indicating kinematic redundancy, this method can be utilized to execute an additional posture task to return the joints to the desired configuration, specifically, the home configuration (upright posture), after push recovery. To address both momentum-based balance control and posture recovery simultaneously, our final control law with control torque $\tau_c \in R^n$ is computed by adding the momentum and posture torques as

$$\tau_c = M(q)\ddot{q}_{momentum} + C(q,\dot{q})\dot{q} + G(q) + M(q)\ddot{q}_{posture} \quad (15)$$

where

$$\ddot{q}_{posture} = (I - J^{\dagger}J)\emptyset_N \quad (16)$$

and $J = \begin{bmatrix} J_x \\ A \end{bmatrix} \in \mathbb{R}^{2\times3}$ is the momentum task (main task) Jacobian, $J^{\dagger}$ denotes the Moore-Penrose inverse of J, and $I \in \mathbb{R}^{3\times3}$ is the identity matrix. The projection matrix $(I - J^{\dagger}J)$ projects any vector onto the null space of J. Therefore, the joint accelerations for the posture recovery $\ddot{q}_{posture}$ have not impact on the momentum task ($J\ddot{q}_{posture} = 0$).

The acceleration $\emptyset_N$ is developed to minimize the errors in joint angular position and velocity. It is defined as:

$$\emptyset_N = -k_q\,|s_q|^{\varepsilon}sgn(s_q) - (\lambda_q\dot{e}_q) \quad (17)$$

where $k_q, \varepsilon, \lambda_q > 0$ and $s_q = \dot{e}_q + \lambda_q e_q$ with e_q being the error in joint angular position.

Fig. 4 shows the block diagram of the proposed push recovery control, which comprises momenta controllers for mitigating external disturbances and posture recovery controller for maintaining an upright posture.

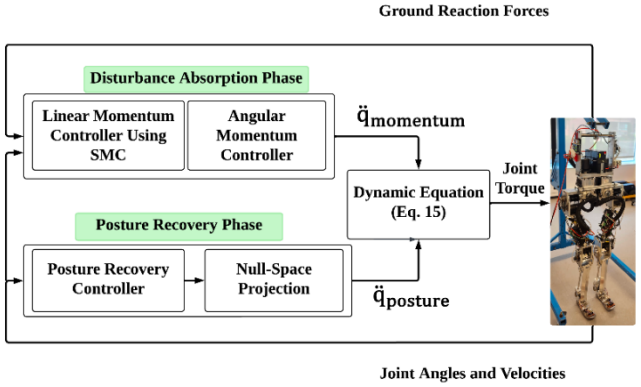

Fig. 4. Proposed push recovery control block diagram

III. RESULTS

A. Performance of Proposed Control using the First Approach of $\dot{H}_{CoM,y}$

To evaluate the efficacy of the proposed push recovery control, an analysis was conducted on the performance of the control algorithm within a simulated environment (Gazebo). A pushing force of 80 N for a duration of 0.1 s is exerted at 0.1 m from the hip joint (waist), as seen in Fig. 5(a). Table I illustrates the control parameters.

TABLE I. CONTROL PARAMETERS

Parameter	λ	k_1	k_3	σ	η	k_H
Value	1.9	0.001	7	1	1	2
Parameter	k_q			λ_q		ϵ
Value	diag([1.95, 1.95, 1.95])			diag([6.1, 6.1, 6.1])		[1, 1, 1]T

The effectiveness in preserving the stability and upright position of the robot is depicted in Fig. 5. The peak of the CoP is measured to be 0.122 m, which is below the maximum limit of 0.18 m, as depicted in Fig. 6(c). The magnitude of the error in the steady state for both the CoP and CoM is 0.0002 m, as depicted in Fig. 6(c). The proposed control also demonstrates apparent effectiveness in mitigating chattering in joint torques, as well as eliminating oscillations, as shown in Fig. 6(a). By minimizing chattering and oscillations in joint torques, the distribution of ground reaction forces at the robot's feet may be precisely controlled. This leads to a more stable position of the CoP and enhances overall balance.

The ankle, knee, and hip joints exhibit maximum torques of 19, 18.1, and 10.4 Nm, respectively. The use of the null-space for posture recovery is depicted in Fig. 6(b), demonstrating the robot's recovery of an upright standing posture with minimal interference to the main controllers, specifically the momenta controllers. Upon analyzing the movement of the joints, it is evident that the knee and hip joints demonstrate forward rotation with angular displacements of -0.11 and -0.57 rad, respectively. In contrast, the ankle joint exhibits an initial backward displacement of 0.03 rad, succeeded by a forward rotation of -0.108 rad. This behavior exhibits similarities to the human response to pushing.

B. *Performance of Proposed Control using the Second Approach of $\dot{H}_{CoM,y}$*

To determine the effectiveness of the Second Approach utilized in the angular momentum controller, a repetition of the test conducted in the first section of the findings was performed. It is noteworthy to remark that this study exclusively considers the positive $\dot{H}_{CoM,y}$ component, which corresponds to the direction of the applied force, in order to counterbalance the external disturbances. Fig. 7 shows the positive $\dot{H}_{CoM,y}$ generated in the Second Approach due to the applied pushing force and the difference between the CoP and CoM positions, as shown in Fig. 8(c).

The peak torques observed in the Second Approach are smaller compared to those in the First Approach, as illustrated in Fig. 8(a). The joint movements demonstrate identical behavior as observed in the First Approach (see Fig. 8(b)). Fig. 8(c) shows that the peak of the CoP is measured at 0.116 m, and the steady state error for both CoP and CoM is 0.001 m. As result, there is an approximate reduction of 6 mm in the CoP peak reducing the CoP fluctuation. This indicates that the Second Approach exhibits improved stability when subjected to a higher pushing force.

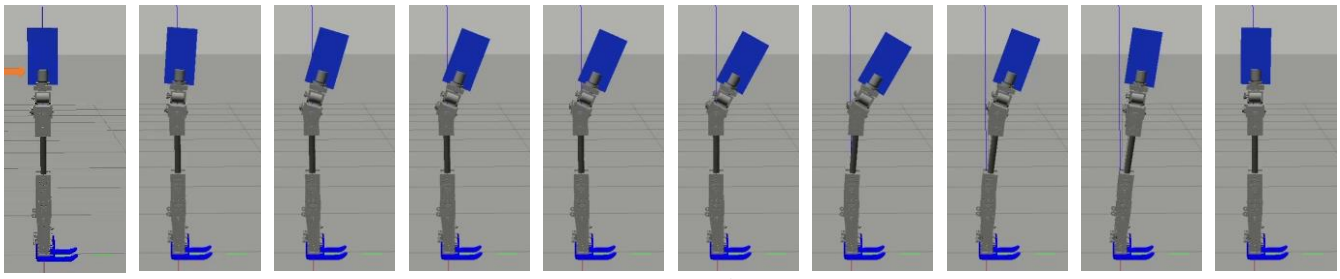

Fig. 5. The simulation response to 80 N at 0.1 m from the hip joint (waist) for 0.1 s with the First Approach (youtube.com/watch?v=zvh4cghN9b8)

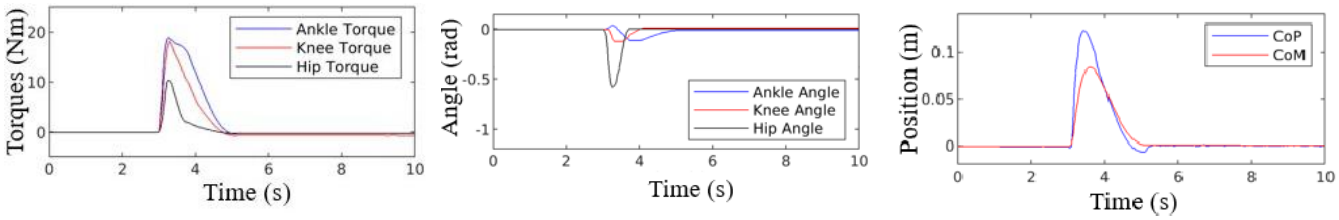

(a) (b) (c)

Fig. 6. The proposed control with the First Approach at a pushing force 80 N at 0.1 m from the hip joint (waist) for 0.1 s (a) Joint Torques, (b) Joint Angles, (c) CoP and CoM positions

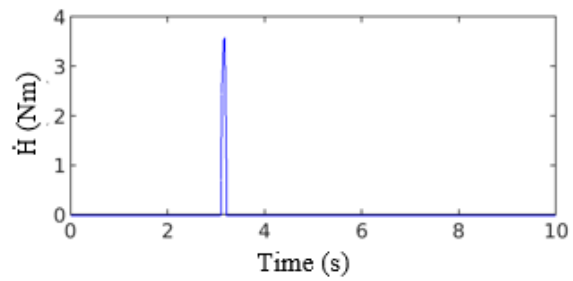

Fig. 7. The desired rate of change of angular momentum defined in (13)

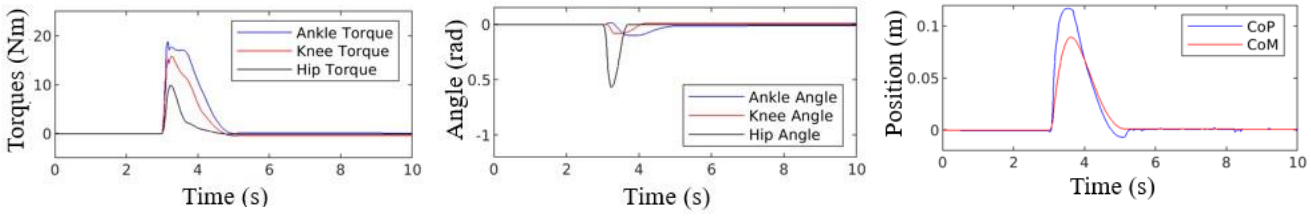

(a) (b) (c)

Fig. 8. The proposed control with the Second Approach at a pushing force 80 N at 0.1 m from the hip joint (waist) for 0.1 s (a) Joint Torques, (b) Joint Angles, (c) CoP and CoM positions

Previous research, as the one conducted in [23], employed a push recovery control system that switches between Disturbance Avoidance Phase and the Posture Recovery Phase. If the robot is pushed during the Posture Recovery Phase, the control system does not initiate the Disturbance Avoidance Phase to stabilize the linear and angular momenta. Disabling the momentum controllers causes the system to function as a stiff pendulum model, with just the joint space control in the Posture Recovery Phase being active. By exclusively relying on the joint space control, the CoP is pushed towards the front of the foot, ultimately resulting in a loss of balance and subsequent fall. As we mentioned earlier, in this study we propose using the null-space method to simultaneously execute both the Disturbance Avoidance Phase and the Posture Recovery Phase. We conducted another experiment by exerting force on the robot on two separate times. The initial push of 70 N is applied with a distance of 0.1 m from the (waist) and a duration of 0.1 s. The second push occurs after one second from the first push, when the robot is returning to an upright position as shown in Fig. 9. Fig. 10 illustrates the ability of our robot (HURON) to maintain balance and an upright posture, even when subjected to two successive pushing forces.

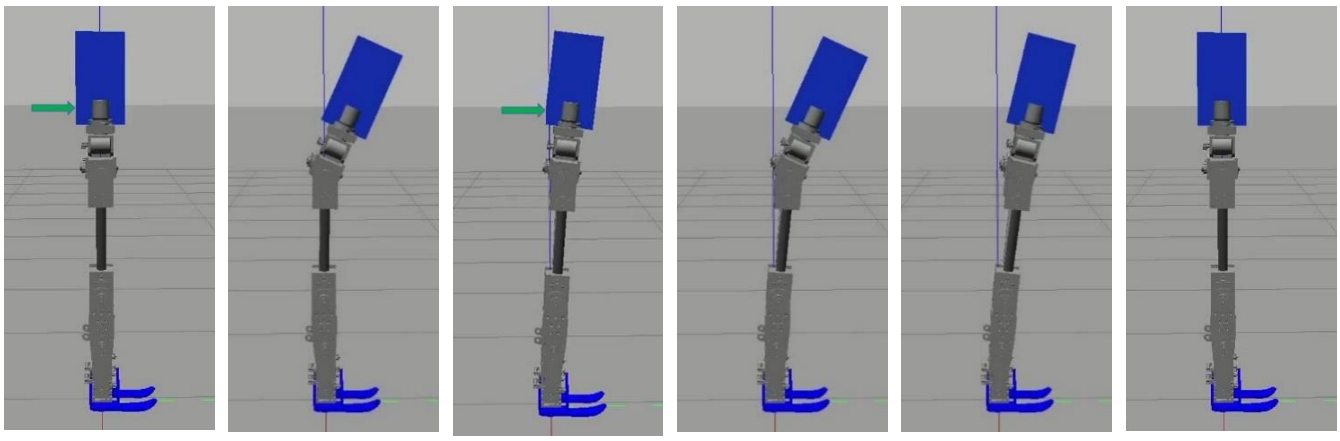

(a) (b) (c) (d) (e) (f)

Fig. 9. The simulation response to 70 N at 0.1 m from the waist for 0.1 s with the Second Approach with two successive pushing forces separated by one second (youtube.com/watch?v=aWAKxNK5P1Y)

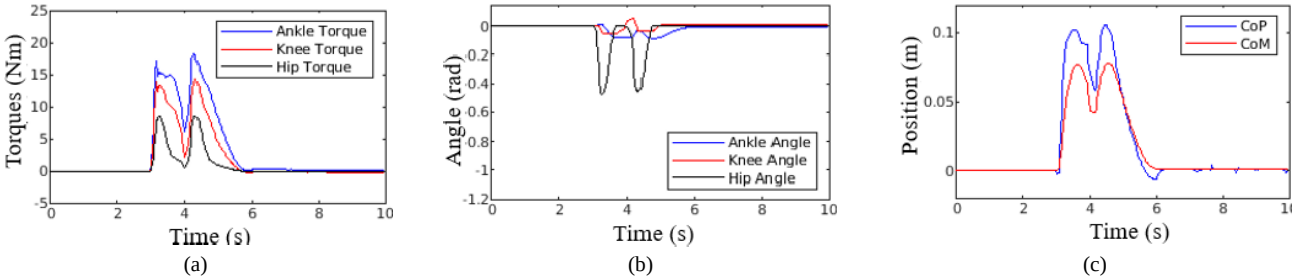

(a) (b) (c)

Fig. 10. The simulation response to 70 N at 0.1 m from the waist for 0.1 s with the Second Approach with two successive pushing forces

C. Comparison with Other Controllers

To compare our proposed push recovery control to previous works, the following four controllers were chosen:

1) Benjamin's controller [75]: A balance controller that enables a humanoid to maintain a standing position while recovering from disturbances. This controller consists of two sub-controllers. The first one is the unconstrained balance controller, which calculates the appropriate torques without imposing any constraints on the position of the CoP. The unconstrained balance controller employed joint space linear quadratic regulator (to drive the joint angles to zero) and CoM controller (to drive the CoM to zero). However, the torque produced by these unrestricted controllers was just utilized to determine the desired position of the CoP. Afterward, the second controller, a decoupled integral controller, was employed to control the position of the CoP precisely. Posture recovery is not used here since CoP does not depend on the torque from posture recovery. Benjamin's controller was chosen to compare our momentum-based control strategy with the CoP integral controller presented in [75].

2) Abdallah et al. [23]: A control technique consists of two phases aiming to maintain balance in a force disturbance. During the reflex phase, the desired momentum change rate was determined to be $\dot{L}_x = -k_2 L_x$ and $\dot{H}_{CoM} = -k_1(CoP_x - CoM_x)$. This phase was responsible for mitigating the destabilizing effects of the disruption. The second phase, known as the recovery phase, was responsible for moving the robot to a stable static posture. The authors of [23] stated that maximizing the potential energy or minimizing the static joint torques $G(q)$ leads to achieving a static stable configuration. We have built the Hessian method, which minimizes the function $G(q)$. The control law for determining the minimal G was established by developing a relationship between the rate of change of G and the joint velocities $\dot{q}$, ($\dot{G} = J(q)\dot{q}$).

3) Constant Power Rate Reaching Law (CPRL)/Constant Rate Reaching Law (CRRL): In the linear momentum controller, we initially replaced the proposed Variable Power Rate Reaching Law with CPRL and subsequently substituted it with CRRL. The controllers were chosen to showcase the chattering issue, the error steady state difficulty, and the efficacy of the proposed SMC in addressing these problems. For the angular momentum controller, we employed the First Approach. We utilized the same posture recovery approach presented in this study.

4) Linear Quadratic Regulator (LQR): The control law is defined as $\tau_{LQR} = -k_{LQR}\begin{bmatrix} q \\ \dot{q} \end{bmatrix}$. The LQR was chosen for comparison because it is a joint space control in which the CoP has no control, showing the importance of CoP control presented by our approach.

In this study, the control settings of the aforementioned controllers were fine-tuned to ensure their best performance on our bipedal robot (HURON) in terms of achieving the minimum CoP distance from the reference frame. We implemented all the controllers within a wide range of forces from low to high forces.

5) CoP Comparison under Low Pushing Force: Fig. 11 illustrates the comparison of CoP fluctuations when using different controllers under a 45 N force applied for 0.1 s at 0.1 m from the waist. LQR and Benjamin's controller [75] show larger CoP fluctuation hence higher CoP peaks at 0.132 m and 0.179 m, respectively. The joint space LQR is anticipated to result in a high CoP position, as its purpose is to drive the joint angles to zero without imposing any restrictions on the CoP position. The robot equipped with the joint space LQR controller exhibits characteristics similar to a stiff inverted pendulum, without the ability to avoid disturbances by generating angular momentum to accelerate forward. The knee joint in Benjamin's work [75] was considered locked, simplifying the robot model through a two-links robot model. This simplification could potentially result in the loss of the ability of the knee joint to absorb disturbances. These, together with ignoring dynamics uncertainties in an ideal simulation environment, might be the possible reasons why Benjamin's controller is not showing satisfactory results in Fig. 11.

Upon performing an analysis of the Constant Rate SMC, it becomes apparent that the joint torques exhibit chattering. Chattering is the consequence of the irregular movement of the CoP caused by the torques applied to the joints. To address the issue of chattering, we utilized a saturation function in combination with the Constant Power Reaching Law. However, this solution led to a steady-state error of 0.005 m in the CoP position. It is obvious that the proposed Variable Power Reaching Law eliminates the chattering issue while providing a small steady-state error of 0.0004 m in the CoP position.

The CoP peaks for the proposed controller (First and Second Approaches), Constant Power Rate SMC, Constant Rate SMC and Abdallah et al. [23] are 0.078 m, 0.073 m, 0.082 m, 0.080 m and 0.078 m, respectively. Although the proposed controller has the lowest CoP value, the reduction compared to Constant Power Rate SMC, Constant Rate SMC and Abdallah et al. [23] is not statistically significant. This is partly due to the similarity in behavior among all three momentum-based controllers when low forces are applied. Another experiment with a high force of 75 N was conducted to distinguish controller behaviors, as described in the next section.

6) CoP Comparison under High Pushing Force: Fig. 12 shows the comparison of CoP fluctuations when using different controllers under a higher pushing force of 75 N applied for 0.1 s. LQR and Benjamin's controllers [75] proved to be ineffective under high-force conditions. The comparison with high pushing force does not include the Constant Rate and Constant Power SMC controllers because they were only used to emphasize the chattering and steady-state error problems. The proposed controller (First Approach), proposed controller (Second Approach), and Abdallah et al. [23] have CoP peaks of 0.120 m, 0.116 m, and 0.167 m, respectively. Given that the proposed push recovery control using the Second Approach yields the smallest CoP fluctuation, we can infer that our robot (HURON) can maintain standing stability even when subjected to large pushing forces. The high CoP position observed in [23] is likely due to the implementation of a simple proportional controller for linear momentum.

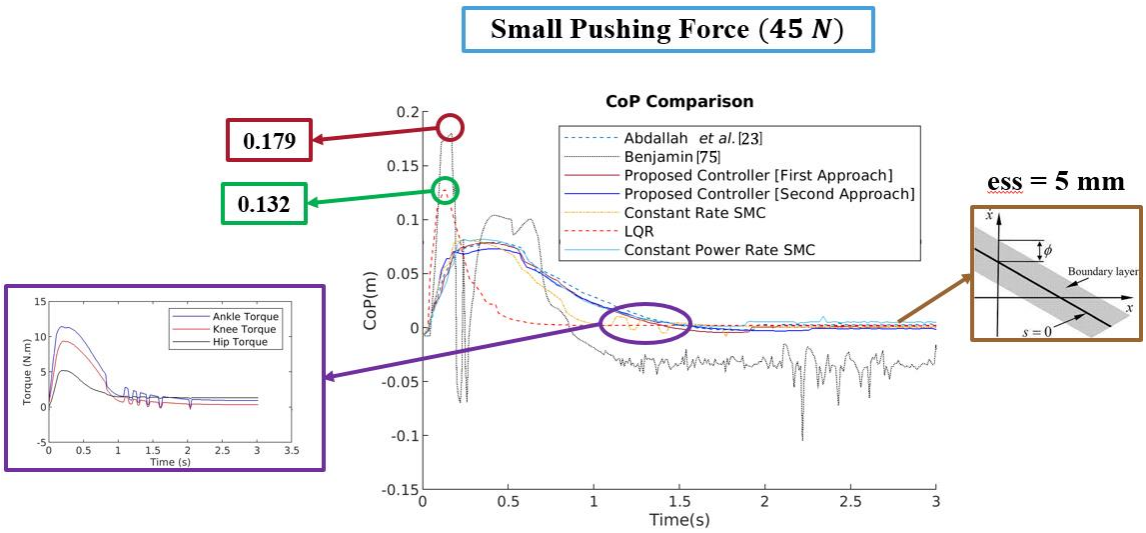

Fig. 11. CoP position comparison is simulated for 3 s with disturbance 45 N applied for 0.1 s

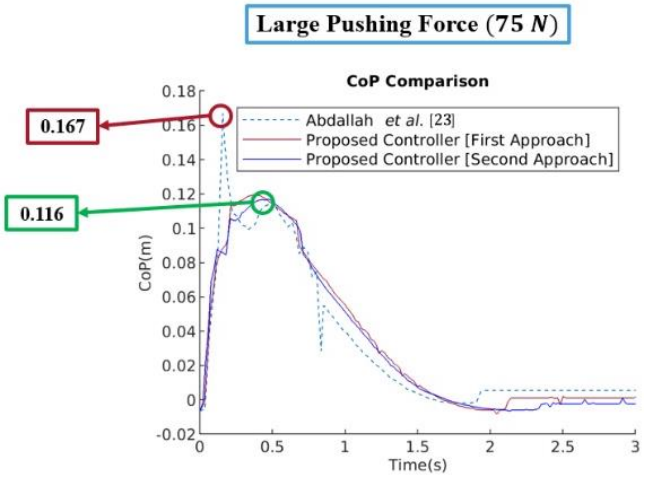

Fig. 12. CoP position comparison is simulated for 3 s with disturbance 75 N applied for 0.1 s.

7) Maximum Force Tolerance: We continued our comparison scenarios by increasing the pushing force to find the maximum force tolerated by each controller before the bipedal robot (HURON) loses stability. The results showed that our proposed control (Second Approach) is able to withstand a force of 117 N applied for 0.1 s making it the most robust among the other controllers. It is important to note that the feet are no longer flat when a pushing force exceeding 117 N is applied, which is considered an unstable state. Comparing with implemented controllers, the maximum force was 52% higher than Abdallah et al. [23], 113% higher than LQR's, and 134% higher than Benjamin's controller [75].

IV. CONCLUSIONS AND FUTURE WORK

This work presented a momentum-based balance control method for bipedal robots when faced with external pushing forces. First, we have developed and validated a Variable Power Rate Reaching Law for Sliding Model Control (SMC) that effectively controls the linear momentum by adapting to changes in the Center of Mass (CoM) states. Hence, the suggested reaching law successfully resolved the problem of chattering and accelerated the rate at which the system reaches the sliding surface. Second, to effectively maintain balance, we have defined the desired rate of change of angular momentum in terms of Center of Pressure (CoP) position, the ground reaction forces, and the desired linear momentum rate of change to counteract the angular momentum induced by the disturbance. This ensured an accurate incorporation of the angular momentum's contribution. Third, our approach proposed utilizing the null-space method for posture recovery without interfering with the primary momentum controllers. The proposed push recovery controller has been implemented and validated on our robot, HURON, within Gazebo, a robust physics-engine simulation environment that delivers results closely resembling real-world conditions with high accuracy. The findings demonstrated the effectiveness of our proposed work in maintaining the stability of HURON under high external forces while addressing the chattering problem. Furthermore, the presented controller enabled our robot to preserve stability in the presence of two successive pushing forces, which is attributed to the employment of null-space method. Comparing with other established controllers, the proposed controller showed superior performance in keeping the CoP within the support polygon with minimum CoP fluctuation, resulting in tolerating higher pushing forces up to 117 N. Based on the findings, we can conclude that HURON has the capability to maintain its standing stability even while it is being subjected to external pushing forces while interacting with its surroundings.

Our future plans include implementing our proposed controller to our manufactured bipedal, HURON, once it is ready for experimental tests. In order to accomplish this, we are developing a robust and open-source software framework constructed using the C++ programming language. This software encompasses the development of a framework and validation of hardware for implementing our push recovery method on the HURON system. Furthermore, the plan involves the derivation of the complex whole-body dynamics of HURON using Roy Featherstone's algorithms, as well as the implementation of the proposed push recovery method in both the sagittal and frontal planes to effectively maintain balance in the presence of external forces acting from various directions.

REFERENCES

[1] X. Yang, H. She, H. Lu, T. Fukuda, and Y. Shen, "State of the Art: Bipedal Robots for Lower Limb Rehabilitation," *Applied Sciences*, vol. 7, no. 11, p. 1182, 2017, doi: 10.3390/app7111182.

[2] K. Yin, Y. Wang, P. Li, K. Dai, Y. Xue, and L. Yang, "Adaptive ankle impedance control for bipedal robotic upright balance," *Expert Systems*, vol. 40, no. 5, p. e13168, 2023, doi: 10.1111/exsy.13168.

[3] Y. Cao, K. Xiang, B. Tang, Z. Ju, and M. Pang, "Design of Muscle Reflex Control for Upright Standing Push-Recovery Based on a Series Elastic Robot Ankle Joint," *Frontiers in Neurorobotics*, vol. 14, p. 20, 2020, doi: 10.3389/fnbot.2020.00020.

[4] E. Chumacero-Polanco and J. Yang, "Effect of disturbances and sensorimotor deficits on the postural robustness of an ankle–hip model of balance on a balance board," *Nonlinear Dynamics*, vol. 99, no. 3, pp. 1959–1973, 2020, doi: 10.1007/s11071-019-05403-w.

[5] P. Morasso, "Integrating ankle and hip strategies for the stabilization of upright standing: An intermittent control model," *Frontiers in Computational Neuroscience*, vol. 16, p. 956932, 2022, doi: 10.3389/fncom.2022.956932.

[6] K. Yin, Y. Xue, Y. Yu, and S. Xie, "Variable Impedance Control for Bipedal Robot Standing Balance Based on Artificial Muscle Activation Model," *Journal of Robotics*, vol. 2021, no. 1, p. 8142161, 2021, doi: 10.1155/2021/8142161.

[7] N. Nernchad and P. Artrit, "Stand balancing strategies for a humanoid robot with slidable floor," *International Journal of Mechanical Engineering and Robotics Research*, vol. 9, no. 4, pp. 511–515, 2020, doi: 10.18178/ijmerr.9.4.511-515.

[8] C. Li, R. Xiong, Q. guo Zhu, J. Wu, Y. liang Wang, and Y. ming Huang, "Push recovery for the standing under-actuated bipedal robot using the hip strategy," *Frontiers of Information Technology and Electronic Engineering*, vol. 16, no. 7, pp. 579–593, 2015, doi: 10.1631/FITEE.14a0230.

[9] M. Shafiee-Ashtiani, A. Yousefi-Koma, M. Shariat-Panahi, and M. Khadiv, "Push recovery of a humanoid robot based on model predictive control and capture point," in *2016 4th International Conference on Robotics and Mechatronics (ICROM)*, pp. 433–438, 2016, doi: 10.1109/ICRoM.2016.7886777.

[10] D. N. Nenchev and A. Nishio, "Experimental validation of ankle and hip strategies for balance recovery with a biped subjected to an impact," *IEEE International Conference on Intelligent Robots and Systems*, vol. 26, no. 5, pp. 4035–4040, 2007, doi: 10.1109/IROS.2007.4399038.

[11] K. Shen, A. Chemori, and M. Hayashibe, "Human-Like Balance Recovery Based on Numerical Model Predictive Control Strategy," *IEEE Access*, vol. 8, pp. 92050–92060, 2020, doi: 10.1109/ACCESS.2020.2995104.

[12] Y. Liu, J. Shen, J. Zhang, X. Zhang, T. Zhu, and D. Hong, "Design and Control of a Miniature Bipedal Robot with Proprioceptive Actuation for Dynamic Behaviors," in *Proceedings - IEEE International Conference on Robotics and Automation*, pp. 8547–8553, 2022, doi: 10.1109/ICRA46639.2022.9811790.

[13] J. Li, Z. Yuan, S. Dong, J. Zhang, and X. Sang, "External force observer aided push recovery for torque-controlled biped robots," *Autonomous Robots*, vol. 46, no. 5, pp. 553–568, 2022, doi: 10.1007/s10514-022-10038-9.

[14] B. J. Stephens and C. G. Atkeson, "Dynamic balance force control for compliant humanoid robots," in *IEEE/RSJ 2010 International Conference on Intelligent Robots and Systems, IROS 2010 - Conference Proceedings*, pp. 1248–1255, 2010, doi: 10.1109/IROS.2010.5648837.

[15] C. Ott, M. A. Roa, and G. Hirzinger, "Posture and balance control for biped robots based on contact force optimization," in *IEEE-RAS International Conference on Humanoid Robots*, pp. 26–33, 2011, doi: 10.1109/Humanoids.2011.6100882.

[16] Z. Wang *et al.*, "A Spring Compensation Method for a Low-Cost Biped Robot Based on Whole Body Control," *Biomimetics*, vol. 8, no. 1, p. 126, 2023, doi: 10.3390/biomimetics8010126.

[17] Y. Yang *et al.*, "Balanced Standing on One Foot of Biped Robot Based on Three-Particle Model Predictive Control," *Biomimetics*, vol. 7, no. 4, p. 244, 2022, doi: 10.3390/biomimetics7040244.

[18] J. Cui, Z. Li, Y. Kuang, and H. Cheng, "Standing balance maintenance by virtual suspension model control for legged robot," *Advances in Mechanical Engineering*, vol. 12, no. 9, p. 1687814020954975, 2020, doi: 10.1177/1687814020954975.

[19] R. Zhang, M. Zhao, and C. L. Wang, "Standing Push Recovery Based on LIPM Dynamics Control for Biped Humanoid Robot," in *2018 IEEE International Conference on Robotics and Biomimetics, ROBIO 2018*, pp. 1732–1737, 2018, doi: 10.1109/ROBIO.2018.8664792.

[20] A. MacChietto, V. Zordan, and C. R. Shelton, "Momentum control for balance," in *ACM Transactions on Graphics*, vol. 28, no. 3, 2009, pp. 1–8. doi: 10.1145/1531326.1531386.

[21] S. Kajita *et al.*, "Resolved Momentum Control: Humanoid Motion Planning Based on the Linear and Angular Momentum," in *IEEE International Conference on Intelligent Robots and Systems*, pp. 1644–1650, 2003, doi: 10.1109/iros.2003.1248880.

[22] S. H. Lee and A. Goswami, "A momentum-based balance controller for humanoid robots on non-level and non-stationary ground," *Autonomous Robots*, vol. 33, no. 4, pp. 399–414, 2012, doi: 10.1007/s10514-012-9294-z.

[23] M. Abdallah and A. Goswami, "A biomechanically motivated two-phase strategy for biped upright balance control," in *Proceedings - IEEE International Conference on Robotics and Automation*, pp. 1996–2001, 2005, doi: 10.1109/ROBOT.2005.1570406.

[24] A. Hofmann, M. Popovic, and H. Herr, "Exploiting angular momentum to enhance bipedal center-of-mass control," in *Proceedings - IEEE International Conference on Robotics and Automation*, pp. 4423–4429, 2009, doi: 10.1109/ROBOT.2009.5152573.

[25] R. Schuller, G. Mesesan, J. Englsberger, J. Lee, and C. Ott, "Online Centroidal Angular Momentum Reference Generation and Motion Optimization for Humanoid Push Recovery," *IEEE Robotics and Automation Letters*, vol. 6, no. 3, pp. 5689–5696, 2021, doi: 10.1109/LRA.2021.3082023.

[26] H. Dai, A. Valenzuela, and R. Tedrake, "Whole-body motion planning with centroidal dynamics and full kinematics," in *IEEE-RAS International Conference on Humanoid Robots*, pp. 295–302, 2015, doi: 10.1109/HUMANOIDS.2014.7041375.

[27] H. J. Lee and J. Y. Kim, "Balance Control Strategy of Biped Walking Robot SUBO-1 Based on Force-Position Hybrid Control," *International Journal of Precision Engineering and Manufacturing*, vol. 22, no. 1, pp. 161–175, 2021, doi: 10.1007/s12541-020-00438-1.

[28] Y. Lu, J. Gao, X. Shi, D. Tian, and Y. Liu, "Sliding balance control of a point-foot biped robot based on a dual-objective convergent equation," *Applied Sciences (Switzerland)*, vol. 11, no. 9, 2021, doi: 10.3390/app11094016.

[29] M. Sobirin and H. Hindersah, "Stability Control for Bipedal Robot in Standing and Walking using Fuzzy Logic Controller," in *Proceedings - 2021 IEEE International Conference on Industry 4.0, Artificial Intelligence, and Communications Technology, IAICT 2021*, pp. 1–7, 2021, doi: 10.1109/IAICT52856.2021.9532516.

[30] M. Popovic, A. Hofmann, and H. Herr, "Angular momentum regulation during human walking: Biomechanics and control," in *Proceedings - IEEE International Conference on Robotics and Automation*, pp. 2405–2411, 2004, doi: 10.1109/robot.2004.1307421.

[31] S. Bakhtiari, M. Razzaghi, and A. Samiee, "A sliding mode controler of hips actuated for passive walking robots," *Journal of Computer & Robotics*, vol. 12, no. 1, pp. 103–112, 2019.

[32] G. Chen, B. Jin, and Y. Chen, "Accurate and robust body position trajectory tracking of six-legged walking robots with nonsingular terminal sliding mode control method," *Applied Mathematical Modelling*, vol. 77, pp. 1348–1372, 2020, doi: 10.1016/j.apm.2019.09.021.

[33] S. A. Ghoreishi, A. F. Ehyaei, and M. Rahmani, "Double hyperbolic sliding mode control of a three-legged robot with actuator constraints," *IET Control Theory and Applications*, vol. 16, no. 15, pp. 1573–1585, 2022, doi: 10.1049/cth2.12326.

[34] A. Sajedifar, M. H. Korayem, and F. Allahverdi, "Dynamic Modelling and Optimal Sliding Mode Control of the Wearable Rehabilitative Bipedal Cable Robot with 7 Degrees of Freedom," *Journal of Intelligent and Robotic Systems: Theory and Applications*, vol. 110, no. 2, pp. 1–16, 2024, doi: 10.1007/s10846-024-02122-2.

[35] M. M. Kakaei and H. Salarieh, "New Robust Control Method Applied to the Locomotion of a 5-Link Biped Robot," *Robotica*, vol. 38, no. 11, pp. 2023–2038, 2020, doi: 10.1017/S0263574719001796.

[36] Y. Gao, W. Wei, X. Wang, D. Wang, Y. Li, and Q. Yu, "Trajectory tracking of multi-legged robot based on model predictive and sliding mode control," *Information Sciences*, vol. 606, pp. 489–511, 2022, doi: 10.1016/j.ins.2022.05.069.

[37] L. Alnufaie, "Fuzzy nonsingular fast terminal sliding mode controller for a robotic system," *International Journal of Advanced and Applied Sciences*, vol. 10, pp. 166–173, 2023, doi: 10.21833/ijaas.2023.10.019.

[38] T. Sun, L. Cheng, Z. Hou, and M. Tan, "Novel sliding-mode disturbance observer-based tracking control with applications to robot manipulators," *Science China Information Sciences*, vol. 64, no. 7, p. 172205, 2021, doi: 10.1007/s11432-020-3043-y.

[39] Z. Anjum, H. Zhou, S. Ahmed, and Y. Guo, "Fixed time sliding mode control for disturbed robotic manipulator," *JVC/Journal of Vibration and Control*, vol. 30, no. 7–8, pp. 1580–1593, 2024, doi: 10.1177/10775463231165094.

[40] C. Jing, H. Zhang, Y. Liu, and J. Zhang, "Adaptive Super-Twisting Sliding Mode Control for Robot Manipulators with Input Saturation," *Sensors*, vol. 24, no. 9, p. 2783, 2024, doi: 10.3390/s24092783.

[41] R. Li, L. Yang, Y. Chen, and G. Lai, "Adaptive Sliding Mode Control of Robot Manipulators with System Failures," *Mathematics*, vol. 10, no. 3, p. 339, 2022, doi: 10.3390/math10030339.

[42] Z. Dachang, H. Pengcheng, D. Baolin, and Z. Puchen, "Adaptive nonsingular terminal sliding mode control of robot manipulator based on contour error compensation," *Scientific Reports*, vol. 13, no. 1, p. 330, 2023, doi: 10.1038/s41598-023-27633-0.

[43] Y. Xu, R. Liu, J. Liu, and J. Zhang, "A novel constraint tracking control with sliding mode control for industrial robots," *International Journal of Advanced Robotic Systems*, vol. 18, no. 4, p. 17298814211029778, 2021, doi: 10.1177/17298814211029778.

[44] Y. Pan, C. Yang, L. Pan, and H. Yu, "Integral Sliding Mode Control: Performance, Modification, and Improvement," *IEEE Transactions on Industrial Informatics*, vol. 14, no. 7, pp. 3087–3096, 2018, doi: 10.1109/TII.2017.2761389.

[45] N. Qiao, L. Wang, M. Liu, and Z. Wang, "The sliding mode controller with improved reaching law for harvesting robots," *Journal of Intelligent and Robotic Systems: Theory and Applications*, vol. 104, no. 1, pp. 1–13, 2022, doi: 10.1007/s10846-021-01536-6.

[46] C. J. Fallaha, M. Saad, H. Y. Kanaan, and K. Al-Haddad, "Sliding-mode robot control with exponential reaching law," *IEEE Transactions on Industrial Electronics*, vol. 58, no. 2, pp. 600–610, 2011, doi: 10.1109/TIE.2010.2045995.

[47] F. Xu, N. An, J. Mao, and S. Yang, "A New Variable Exponential Power Reaching Law of Complementary Terminal Sliding Mode Control," *Complexity*, vol. 2020, no. 1, p. 8874813, 2020, doi: 10.1155/2020/8874813.

[48] H. Wang, X. Zhao, and Y. Tian, "Trajectory tracking control of XY table using sliding mode adaptive control based on fast double power reaching law," *Asian Journal of Control*, vol. 18, no. 6, pp. 2263–2271, 2016, doi: 10.1002/asjc.1322.

[49] Z. Kang, H. Yu, and C. Li, "Variable-parameter double-power reaching law sliding mode control method*," *Automatika*, vol. 61, no. 3, pp. 345–351, 2020, doi: 10.1080/00051144.2020.1757965.

[50] L. Wang *et al.*, "A sliding mode control method based on improved reaching law for superbuck converter in photovoltaic system," *Energy Reports*, vol. 8, pp. 574–585, 2022, doi: 10.1016/j.egyr.2022.03.159.

[51] V. Nayak and S. K. Gudey, "An Enhanced Exponential Reaching Law Based Sliding Mode Control Strategy for a Three Phase UPS System," *Serbian Journal of Electrical Engineering*, vol. 17, no. 3, pp. 313–336, 2020, doi: 10.2298/SJEE2003313N.

[52] B. Jiang, J. Li, and S. Yang, "An improved sliding mode approach for trajectory following control of nonholonomic mobile AGV," *Scientific Reports*, vol. 12, no. 1, p. 17763, 2022, doi: 10.1038/s41598-022-22697-w.

[53] S. Li, H. Wang, H. Li, and C. Yang, "PMSM sliding mode control based on novel reaching law and extended state observer," *Advances in Mechanical Engineering*, vol. 14, no. 8, p. 16878132221119960, 2022, doi: 10.1177/16878132221119960.

[54] Y. Wang, Y. Feng, X. Zhang, J. Liang, and X. Cheng, "New reaching law control for permanent magnet synchronous motor with extended disturbance observer," *IEEE Access*, vol. 7, pp. 186296–186307, 2019, doi: 10.1109/ACCESS.2019.2956846.

[55] H. Armghan, M. Yang, N. Ali, A. Armghan, and A. Alanazi, "Quick reaching law based global terminal sliding mode control for wind/hydrogen/battery DC microgrid," *Applied Energy*, vol. 316, p. 119050, 2022, doi: 10.1016/j.apenergy.2022.119050.

[56] Y. Zhao, M. Noori, and W. A. Altabey, "Reaching law based sliding mode control for a frame structure under seismic load," *Earthquake Engineering and Engineering Vibration*, vol. 20, no. 3, pp. 727–745, 2021, doi: 10.1007/s11803-021-2049-0.

[57] A. G. Iyer, J. Samantaray, S. Ghosh, A. Dey, and S. Chakrabarty, "Sliding Mode Control Using Power Rate Exponential Reaching Law for Urban Platooning," *IFAC-PapersOnLine*, vol. 55, no. 1, pp. 516–521, 2022, doi: 10.1016/j.ifacol.2022.04.085.

[58] S. Wang, C. Jiang, Q. Tu, and C. Zhu, "Sliding mode control with an adaptive switching power reaching law," *Scientific Reports*, vol. 13, no. 1, p. 16155, 2023, doi: 10.1038/s41598-023-43304-6.

[59] P. Leśniewski and A. Bartoszewicz, "Reaching law based sliding mode control of sampled time systems," *Energies*, vol. 14, no. 7, p. 1882, 2021, doi: 10.3390/en14071882.

[60] W. Gao and J. C. Hung, "Variable Structure Control of Nonlinear Systems: A New Approach," *IEEE Transactions on Industrial Electronics*, vol. 40, no. 1, pp. 45–55, 1993, doi: 10.1109/41.184820.

[61] M. Mori and M. Sugihara, "The double-exponential transformation in numerical analysis," *Journal of Computational and Applied Mathematics*, vol. 127, no. 1–2, pp. 287–296, 2001, doi: 10.1016/S0377-0427(00)00501-X.

[62] T. Ooura and M. Mori, "A robust double exponential formula for Fourier-type integrals," *Journal of Computational and Applied Mathematics*, vol. 112, no. 1–2, pp. 229–241, 1999, doi: 10.1016/S0377-0427(99)00223-X.

[63] L. Aceto and P. Novati, "Exponentially Convergent Trapezoidal Rules to Approximate Fractional Powers of Operators," *Journal of Scientific Computing*, vol. 91, no. 2, p. 55, 2022, doi: 10.1007/s10915-022-01837-4.

[64] G. Notomista, S. Mayya, M. Selvaggio, M. Santos, and C. Secchi, "A Set-Theoretic Approach to Multi-Task Execution and Prioritization," in *Proceedings - IEEE International Conference on Robotics and Automation*, pp. 9873–9879, 2020, doi: 10.1109/ICRA40945.2020.9196741.

[65] S. Zhang, S. Cheng, and Z. Jin, "A Control Method of Mobile Manipulator Based on Null-Space Task Planning and Hybrid Control," *Machines*, vol. 10, no. 12, p. 1222, 2022, doi: 10.3390/machines10121222.

[66] R. S. Jamisola and R. G. Roberts, "An approach to drastically reduce the required legs DOFs for bipedal robots and lower-limb exoskeletons," *Robotica*, vol. 40, no. 4, pp. 1207–1221, 2022, doi: 10.1017/S0263574721001090.

[67] N. Wilhelm, R. Burgkart, J. Lang, C. Micheler, and C. von Deimling, "Exploiting null space potentials to control arm robots compliantly performing nonlinear tactile tasks," *International Journal of Advanced Robotic Systems*, vol. 16, no. 6, p. 1729881419885473, 2019, doi: 10.1177/1729881419885473.

[68] B. Taner and K. Subbarao, "Modeling of Cooperative Robotic Systems and Predictive Control Applied to Biped Robots and UAV-UGV Docking with Task Prioritization," *Sensors*, vol. 24, no. 10, p. 3189, 2024, doi: 10.3390/s24103189.

[69] K. Fan, Y. Liu, B. Huo, L. Yang, Z. Wu, and H. Yu, "Cascaded ESO based multi-task priority tracking and null-space compliance control for redundant robots," *Control Engineering Practice*, vol. 141, p. 105710, 2023, doi: 10.1016/j.conengprac.2023.105710.

[70] M. Khatib, K. Al Khudir, and A. De Luca, "Task Priority Matrix at the Acceleration Level: Collision Avoidance under Relaxed Constraints," *IEEE Robotics and Automation Letters*, vol. 5, no. 3, pp. 4970–4977, 2020, doi: 10.1109/LRA.2020.3004771.

[71] P. Hsu, J. Mauser, and S. Sastry, "Dynamic control of redundant manipulators," *Journal of Robotic Systems*, vol. 6, no. 2, pp. 133–148, 1989, doi: 10.1002/rob.4620060203.

[72] B. Siciliano and J.-J. E. Slotine, "A general framework for managing multiple tasks in highly redundant robotic systems," in *proceeding of 5th International Conference on Advanced Robotics*, 2002, pp. 1211–1216 vol.2. doi: 10.1109/icar.1991.240390.

[73] Y. Nakamura, H. Hanafusa, and T. Yoshikawa, "Task-Priority Based Redundancy Control of Robot Manipulators.," *International Journal of*

Robotics Research, vol. 6, no. 2, pp. 3–15, 1987, doi: 10.1177/027836498700600201.

[74] J. M. Hollerbach and K. C. Suh, "Redundancy resolution of manipulators through torque optimization," *Proceedings - IEEE International Conference on Robotics and Automation*, vol. 3, no. 4, pp. 1016–1021, 1985, doi: 10.1109/ROBOT.1985.1087285.

[75] B. Stephens, "Integral control of humanoid balance," in *IEEE International Conference on Intelligent Robots and Systems*, pp. 4020–4027, 2007, doi: 10.1109/IROS.2007.4399407.

[76] O. Khatib, "Real-time obstacle avoidance for manipulators and mobile robots," *Proceedings - IEEE International Conference on Robotics and Automation*, vol. 5, no. 1, pp. 500–505, 1985, doi: 10.1109/ROBOT.1985.1087247.

[77] O. Khatib, "A Unified Approach for Motion and Force Control of Robot Manipulators: The Operational Space Formulation," *IEEE Journal on Robotics and Automation*, vol. 3, no. 1, pp. 43–53, 1987, doi: 10.1109/JRA.1987.1087068.

[78] O. KHATIB, L. SENTIS, J. PARK, and J. WARREN, "Whole-Body Dynamic Behavior and Control of Human-Like Robots," *International Journal of Humanoid Robotics*, vol. 1, no. 1, pp. 29–43, 2004, doi: 10.1142/S0219843604000058.

[79] L. Sentis and O. Khatib, "Prioritized multi-objective dynamics and control of robots in human environments," in *2004 4th IEEE-RAS International Conference on Humanoid Robots*, pp. 764–780, 2004, doi: 10.1109/ichr.2004.1442684.

[80] J. Nakanishi, R. Cory, M. Mistry, J. Peters, and S. Schaal, "Operational space control: A theoretical and empirical comparison," *International Journal of Robotics Research*, vol. 27, no. 6, pp. 737–757, 2008, doi: 10.1177/0278364908091463.